Electronic Supplementary Information

Metal-Organic Frameworks-Templated Synthesis of Sulfur-Doped Core-Sheath Nanoarrays and Nanoporous Carbons for Flexible All-Solid-State Asymmetric Supercapacitors

Simeng Dai, Yan Yuan, Jiangsheng Yu, Jian Tang, Jie Zhou*, and Weihua Tang*

Key Laboratory of Soft Chemistry and Functional Materials, Ministry of Education, Nanjing University of Science and Technology, Nanjing 210094, People's Republic of China

*Corresponding author. Tel: (86)-25-8431-7311. E-mail: fnzhoujie@njust.edu.cn and whtang@njust.edu.cn

Table of Contents

1. Experimental

1.1. Chemicals and Materials

Carbon cloth (CC, WOS1002) was provided by Ce-Tech Co., Ltd. (Taiwan). Cobalt nitrate hexahydrate [$Co(NO_3)_2 \cdot 6H_2O$], ammonium fluoride, urea, thioacetamide and 2-methylimidazole were purchased from Energy Chemical Co., Ltd. (Shanghai, China). Methanol, ethanol, acetone, nitric acid (68 wt%) and hydrochloric acid (12 mol/L) were purchased from Titan Scientific Co., Ltd. (Shanghai, China). DI-water was obtained from a Millipore Q water purification system. All reagents were of analytical grade and used directly without further purification.

1.2 Preparation of CC@CoO NAs on CC

Prior to the growth of CoO nanowires, the CC substrates was cleaned by sequential ultrasonic treatment in acetone, DI-water and ethanol for 2 h, respectively. Afterwards, CC substrates were activated in nitric acid for 4 h and dried in vacuum. The vertical growth of CoO nanowires on CC was achieved via a hydrothermal method and annealing process.[S1] Typically, $Co(NO_3)_2 \cdot 6H_2O$ (582 mg, 2 mmol), urea (600 mg, 10 mmol) and ammonium fluoride (296 mg, 8 mmol) were dissolved in DI-water (36 mL), then a piece of clean CC substrate (2 cm × 5 cm) was immersed into this homogeneous solution. The mixture was transferred into a Teflon-lined stainless steel autoclave (50 mL), which was sealed and maintained at 120 ^oC for 10 h. The CC substrate was taken out and washed with deionized water for at least three times. After dried in vacuum, the CC substrate was further annealed at 350 ^oC in N_2 atmosphere for 1 h, with a heating rate of 5 ^oC min^{-1}. The obtained hybrid was denoted as CC@CoO and the area mass loading was 0.975 mg cm^{-2}.

1.3 Preparation of CC@CoO@Co_3O_4

The conversion of ZIF-67 to Co_3O_4 was performed via an annealing process.[S2] Typically, The as-prepared CC@CoO@ZIF-67 was firstly annealed in N_2 atmosphere at 500 ^oC for 0.5 h with a ramp rate of 2 ^oC min^{-1}. Then, the temperature was decreased from 500 ^oC to 350 ^oC with a decrease speed of 5 °C min^{-1}. The sample was further annealed in the air for 2 h at 350 ^oC. The resulted sample was denoted as CC@CoO@Co_3O_4 with an average mass loading of about 1.110 mg cm^{-2}.

1.4 Calculation for electrochemical measurements

For three electrodes system, the areal specific capacitance (C_a) of cathode and anode were calculated from Eq. (1):[S3]

$$C_a = \frac{I \Delta t}{A \Delta V} \tag{1}$$

where I is the discharge current, Δt is the discharge time, A is electrode area, ΔV is the voltage drop upon discharge.

For two electrodes system, the charge stored in cathode (Q^+) and anode (Q^-) should be balanced, i.e., $Q^+=Q^-$. The charge stored in electrode can thus be expressed with the areal specific capacitance (C_a), the potential window (ΔV) and the area of each electrode (A) by Eq. (2)-(3):

$$Q = C_a \times \Delta V \times A \tag{2}$$

$$C_a^+ \times \Delta V^+ \times A^+ = C_a^- \times \Delta V^- \times A^- \tag{3}$$

where C_a^+ and C_a^- refers to the C_a for cathode and anode, respectively; $\Delta V^+ and \Delta V^-$ for the potential window of cathode and anode; $A^+ and\ A^-$ for the area of cathode and anode, respectively.

The volumetric specific capacitance (C_v), energy density (E) and power density (P) of asymmetric supercapacitor were calculated using Eq. (4)~(6):

$$C_v = \frac{I \Delta t}{v \Delta V} \tag{4}$$

$$E = \frac{1}{2} C V^2 \tag{5}$$

$$P = \frac{E}{\Delta t} \tag{6}$$

where I is the discharge current, ΔV is the voltage drop upon discharge by excluding the IR drops, Δt is the discharge time and v is the volume of the device.[S3] In our case, the thickness of as asymmetric device is determined to be 0.075 cm using an electronic calliper.

1.5. Materials Characterization

The morphology of the as-prepared nanomaterials was evaluated by field emission scanning electron microscope (FESEM, J Hitachi S-4800 at an accelerating voltage of 10 kV). The transmission electron microscope (TEM) images were obtained from FEI Tecnai-12 at an accelerating voltage of 120 kV. High-resolution transmission electron microscopy (HR-TEM) was performed on a FEI Tecnai F30 at an accelerating voltage of 80 kV. X-ray diffraction (XRD) patterns were recorded on a Bruker D8 Advance Diffractometer with a Cu Ka radiation of 1.54 Å at 40 kV. X-ray photoelectron spectroscopy (XPS) analysis were carried out on a Thermo ESCALAB 250 X-ray photoelectron spectrometer. Raman spectroscopy (RM 2000 microscopic confocal Raman spectrometer) was performed by employing a 514 nm laser beam. The pore volume and surface area of electrode were measured by Brunauer-Emmet-Teller (BET) surface analyzer (Micromeritics, ASAP 2020) at 77 K.

2. Results and discussion

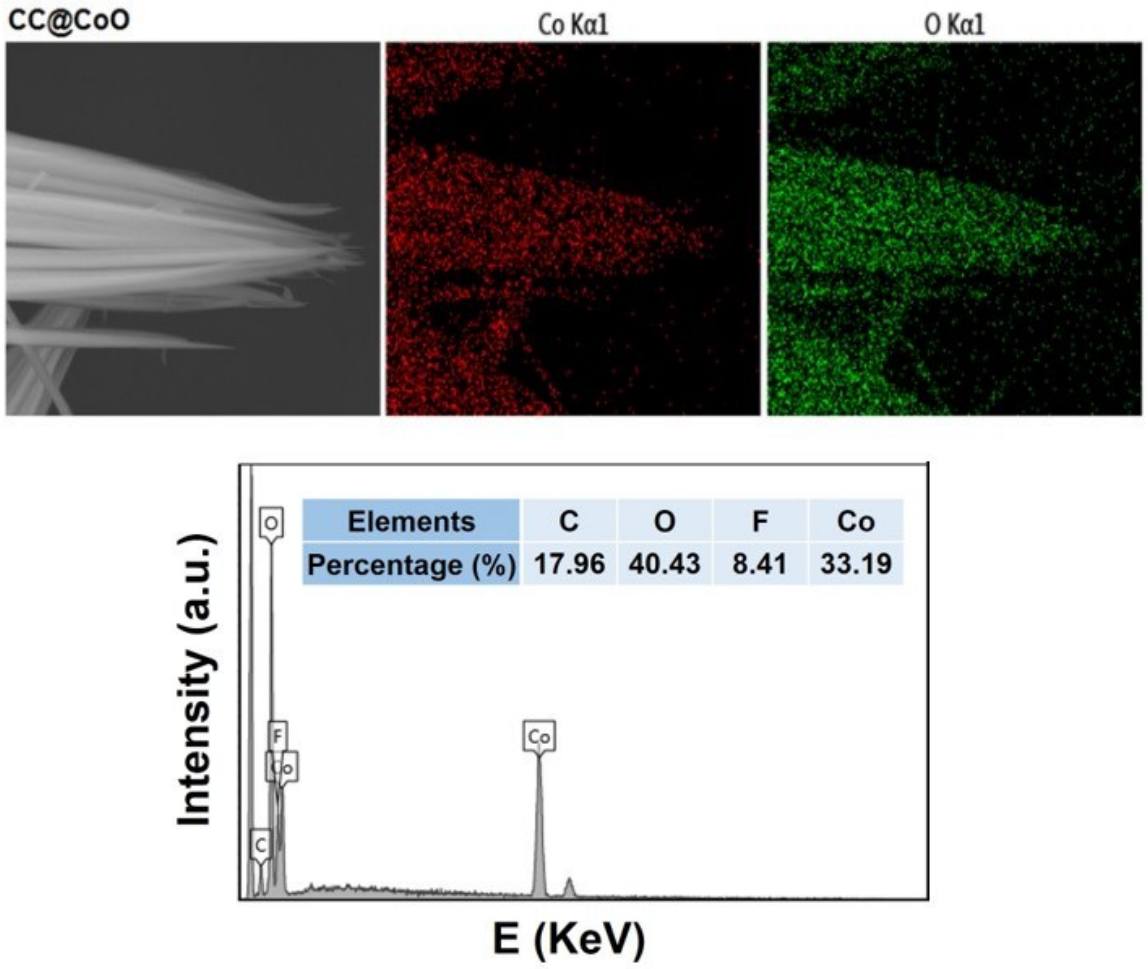

Figure S1. EDS mapping images of corresponding elements for CC@CoO.

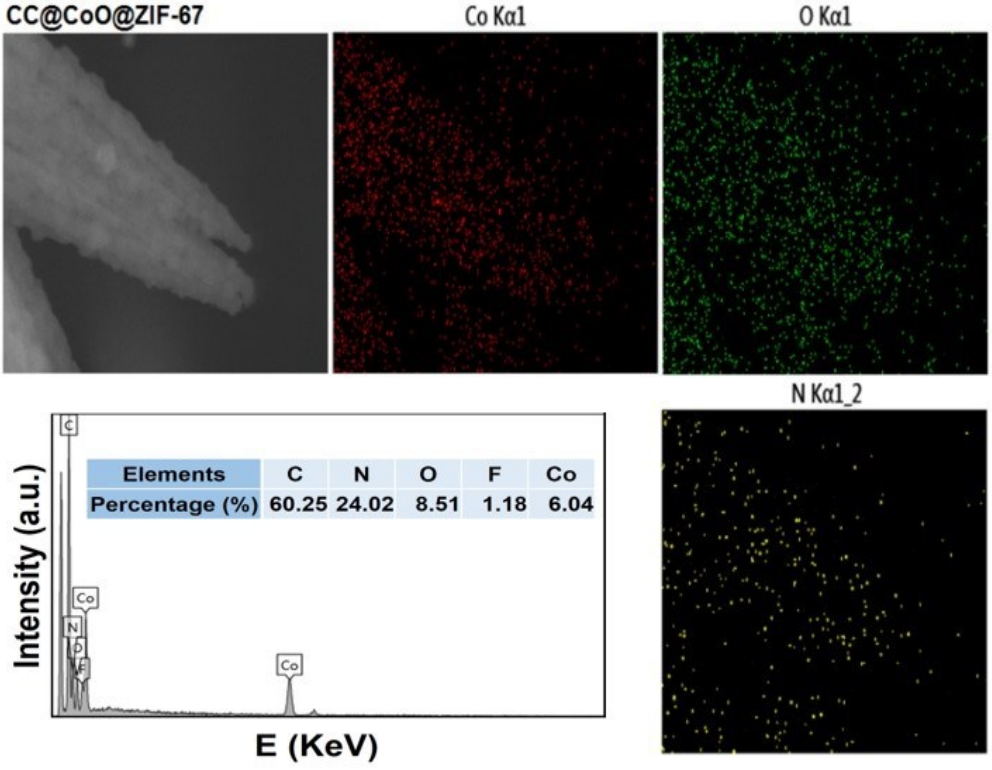

Figure S2. EDS mapping images of corresponding elements for CC@CoO@ZIF-67.

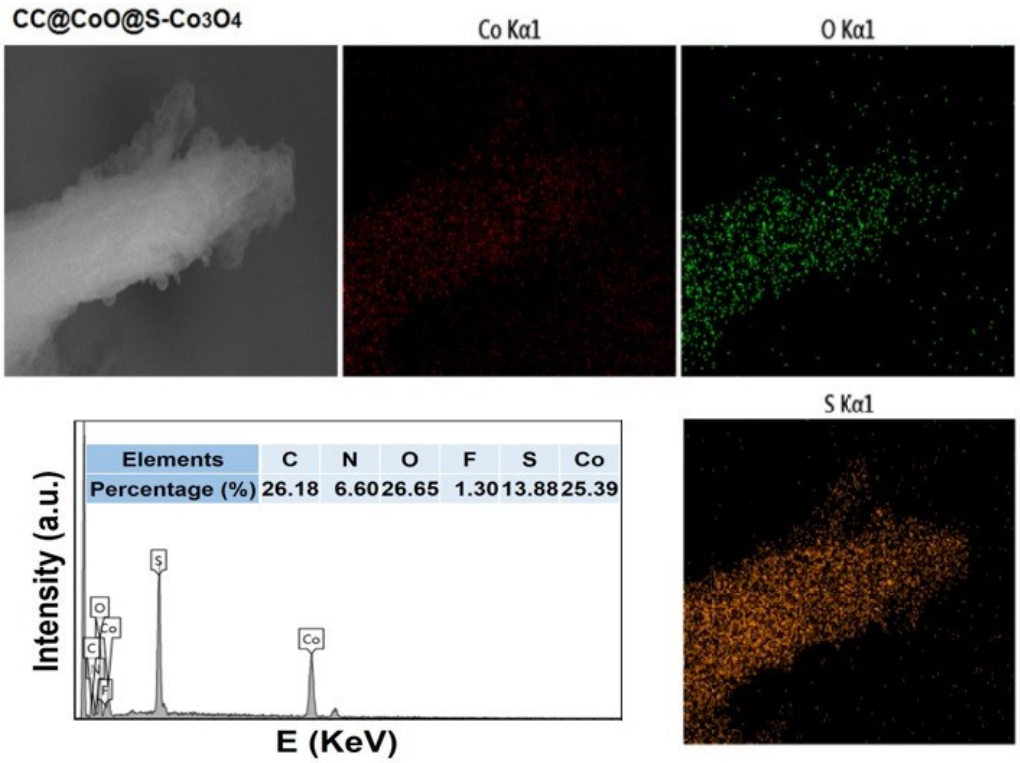

Figure S3. EDS mapping images of corresponding elements for CC@CoO@S-Co_3O_4.

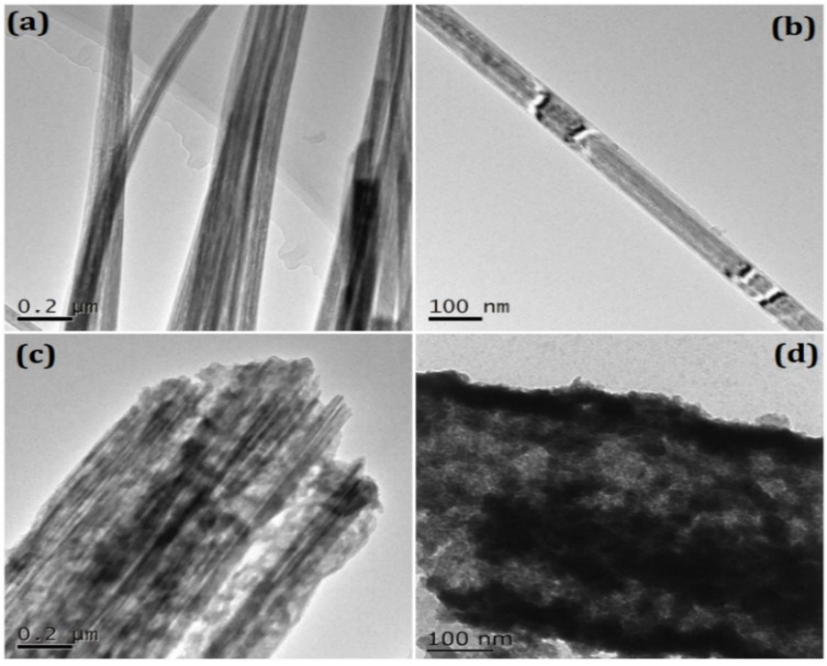

Figure S4. TEM images of (a,b) CoO and (c,d) CoO@S-Co_3O_4 at a scan bar of 0.2 μm and 100 nm.

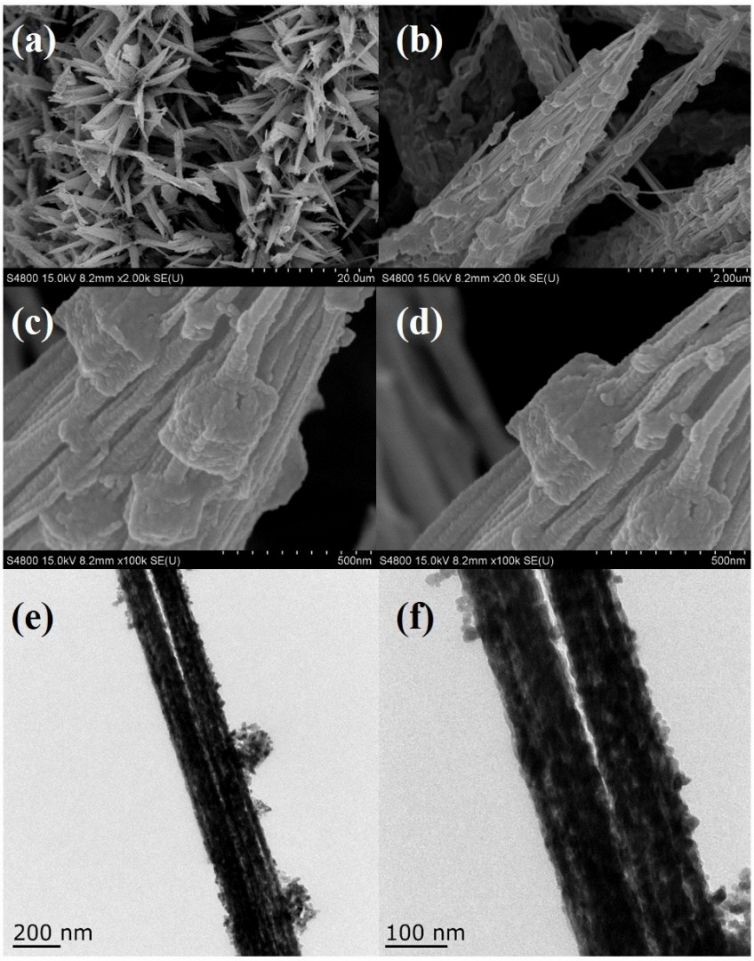

Figure S5. FESEM images (a-d) and TEM images (e-f) of CC@CoO@Co_3O_4.

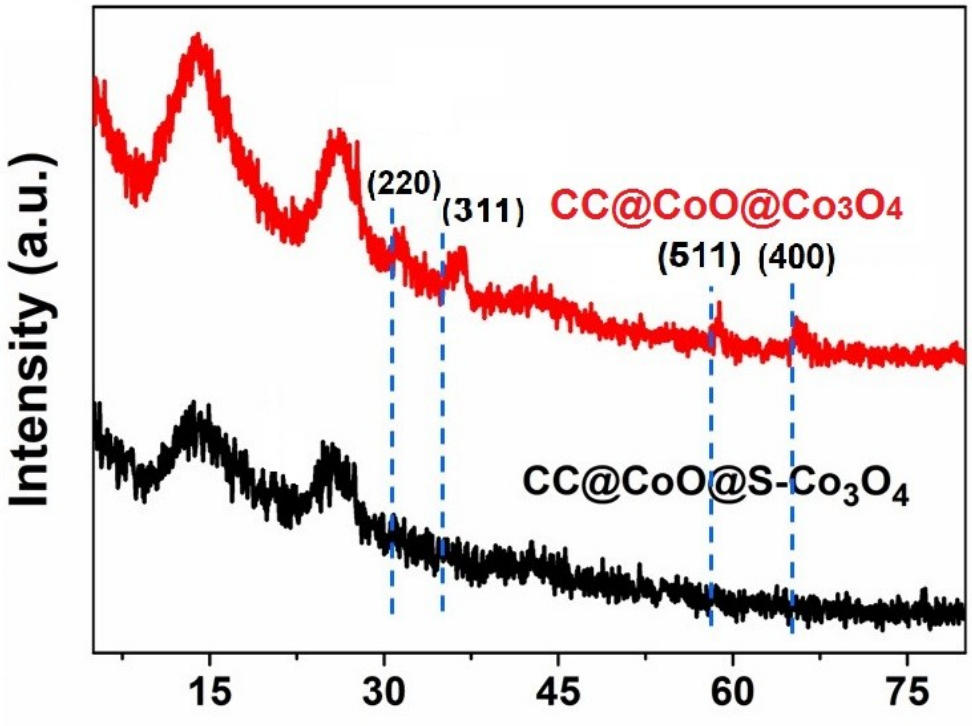

Figure S6. Comparison XRD patterns of CC@CoO@S-Co_3O_4 and CC@CoO@Co_3O_4.

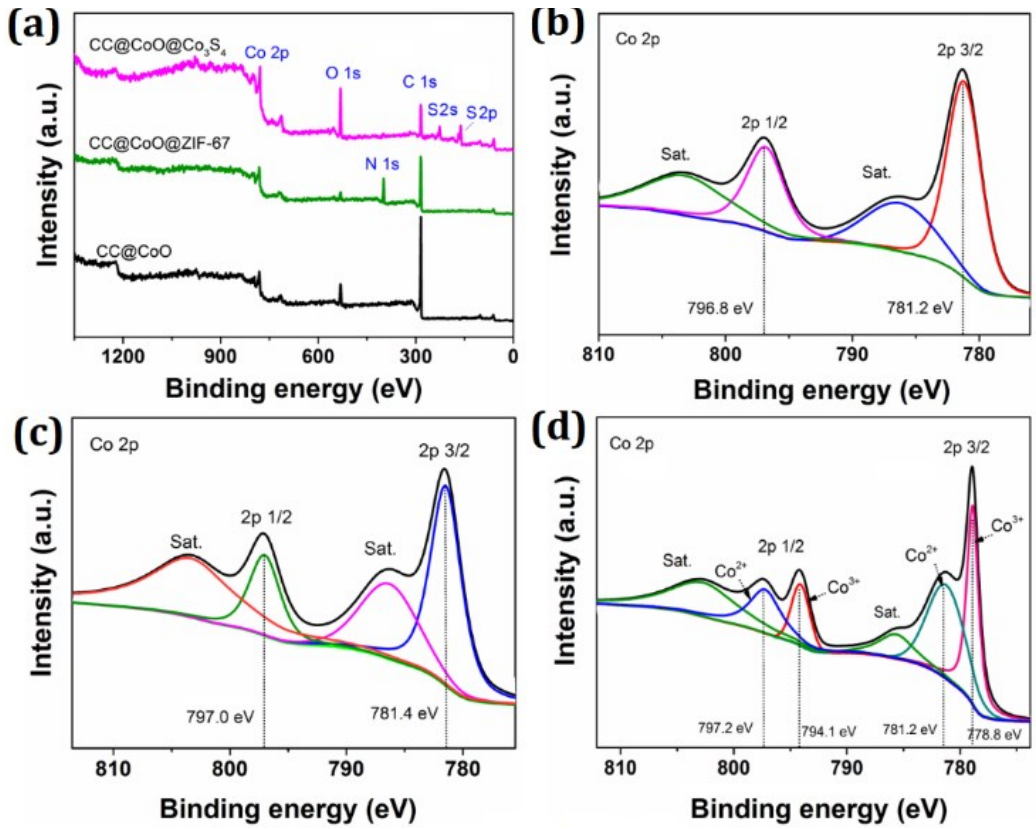

Figure S7. (a) Full survey XPS spectra and according high-resolution regions of Co 2p for (b-d) CC@CoO, CC@CoO@ZIF-67 and CC@CoO@S-Co_3O_4, respectively.

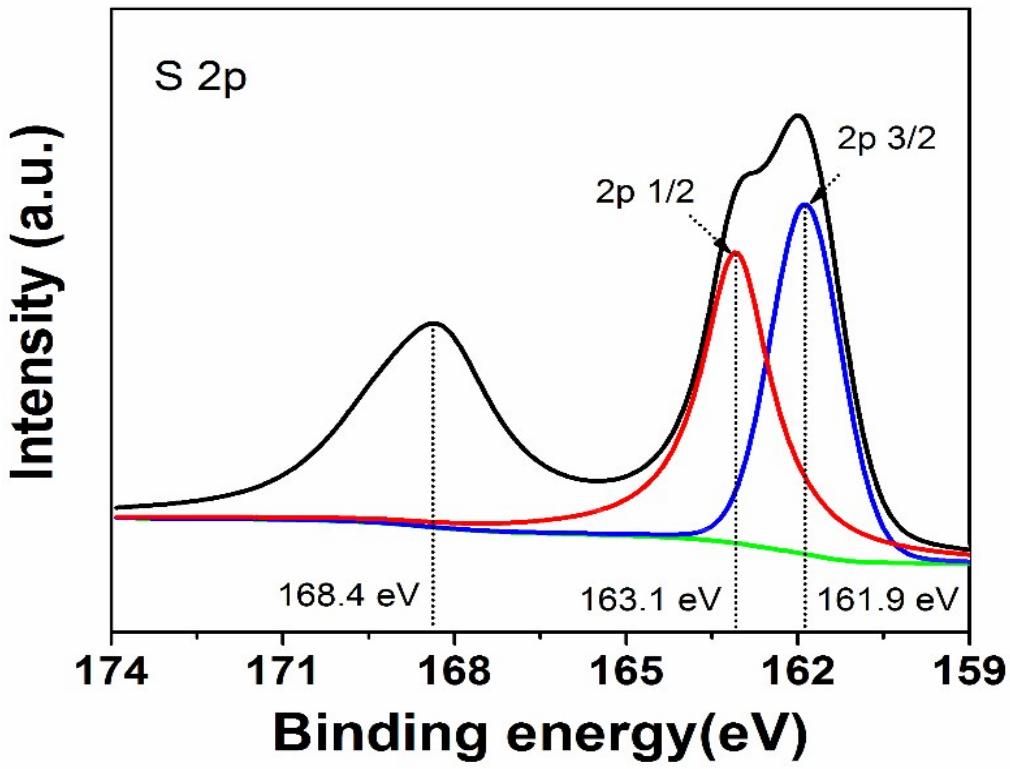

Figure S8. High-resolution regions of S 2p for CC@CoO@S-Co_3O_4.

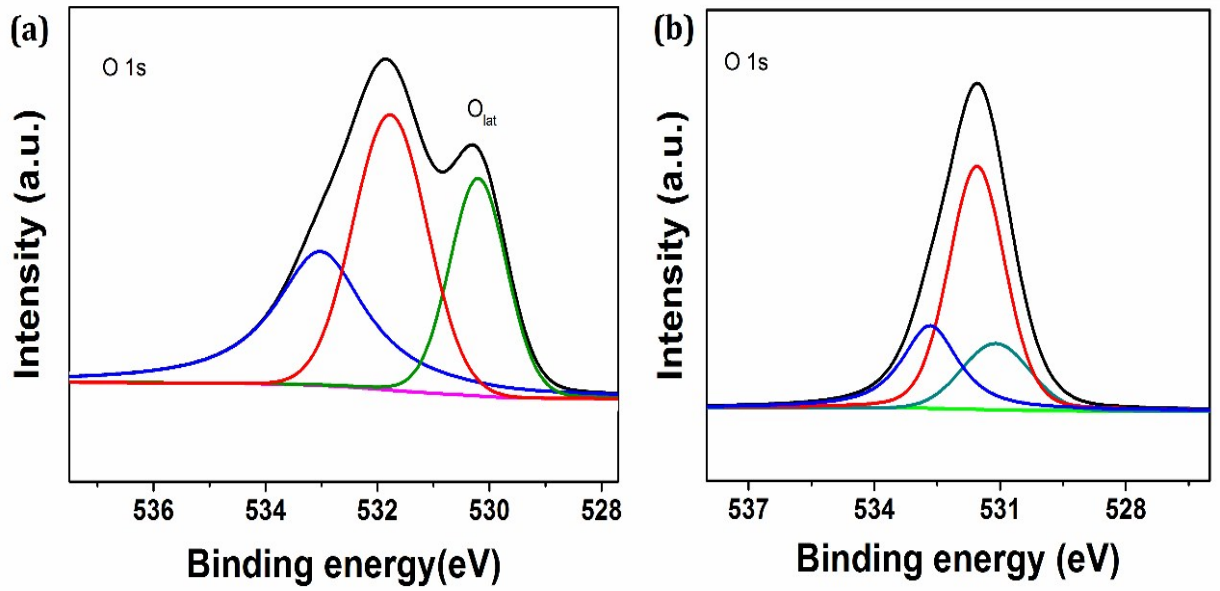

Figure S9. High-resolution regions of O 1s for (a) CC@CoO and (b) CC@CoO@S-Co_3O_4.

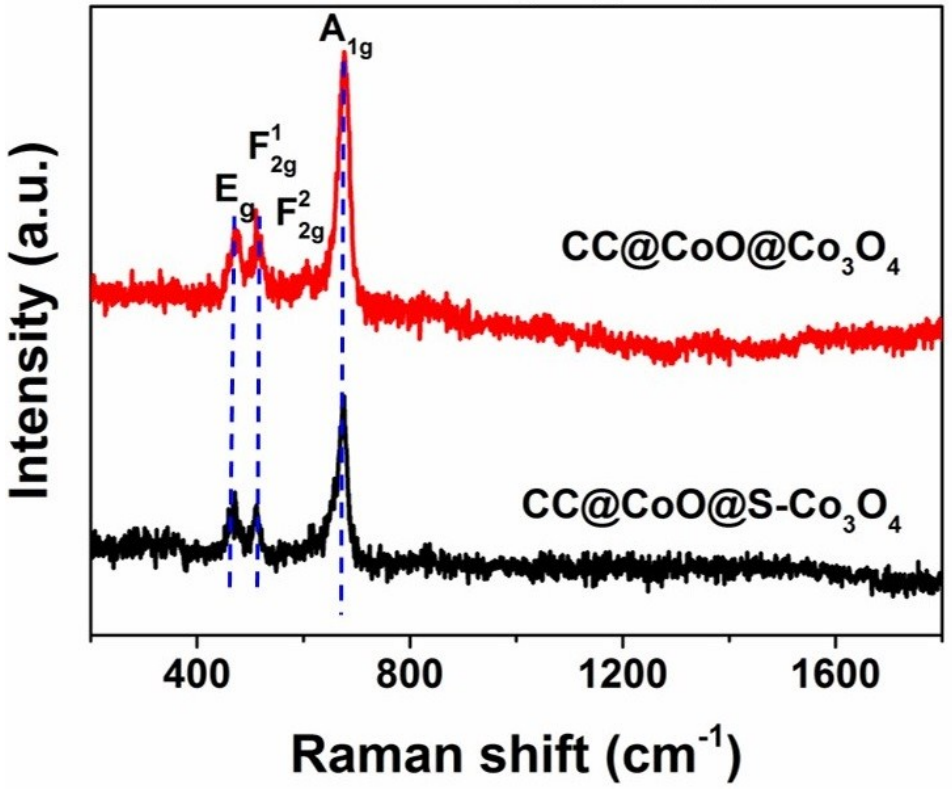

Figure S10. Raman spectra of CC@CoO@S-Co_3O_4 and CC@CoO@Co_3O_4.

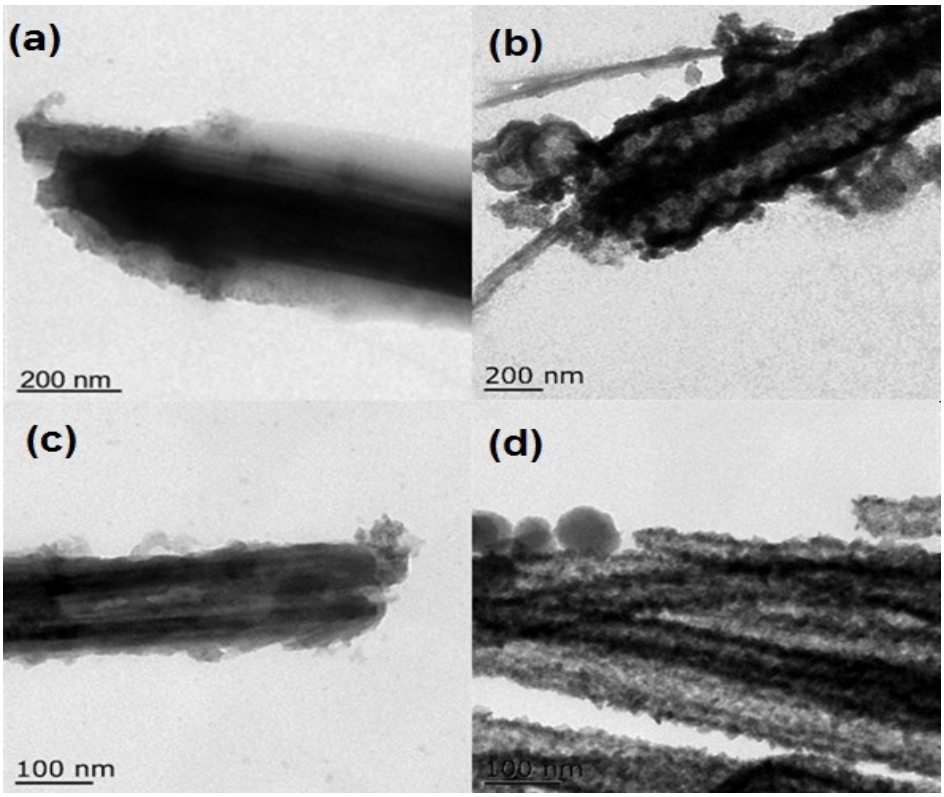

Figure S11. TEM images of CC@CoO@S-Co_3O_4 at different hydrothermal time of (a) 1.5 h, (b) 2.5 h, (c) 3.5 h and (d) 5 h, respectively.

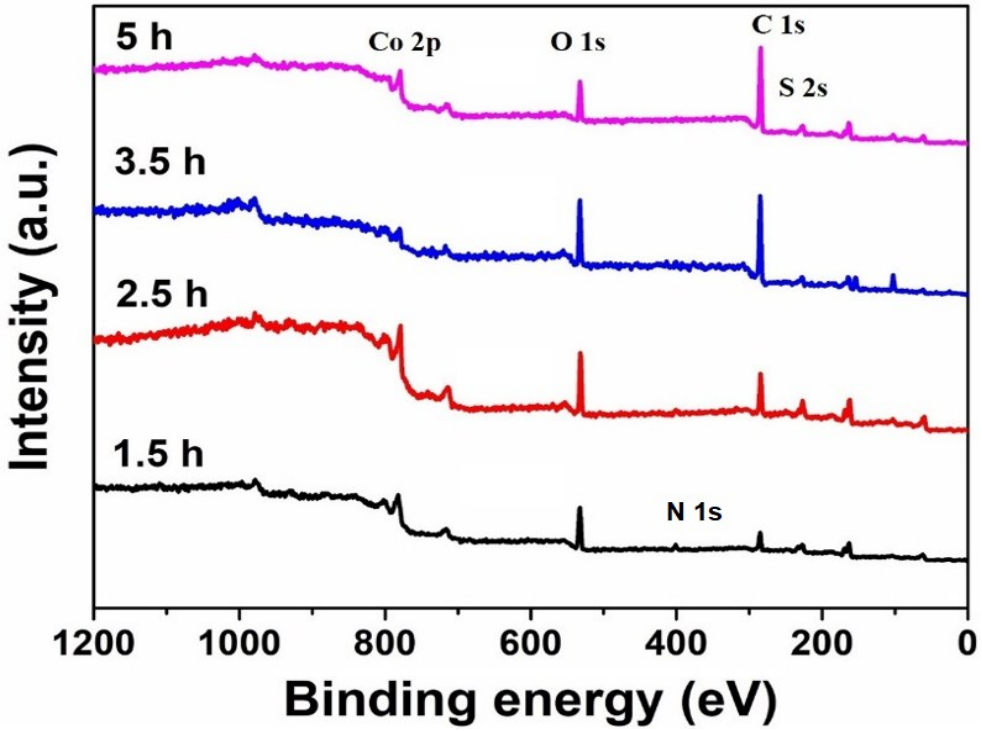

Figure S12. Full survey XPS spectra for CC@CoO@S-Co_3O_4 obtained at different hydrothermal time.

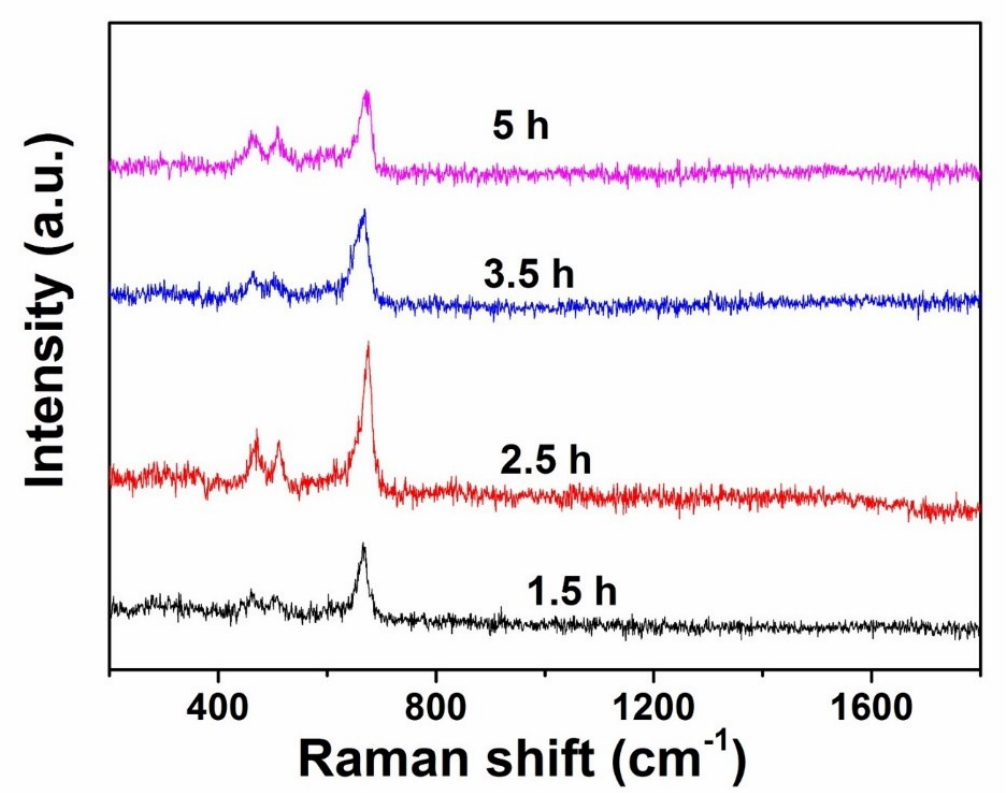

Figure S13. Raman spectra for CC@CoO@S-Co_3O_4 obtained from different thermal time of 1.5 h, 2.5 h, 3.5h and 5h, respectively.

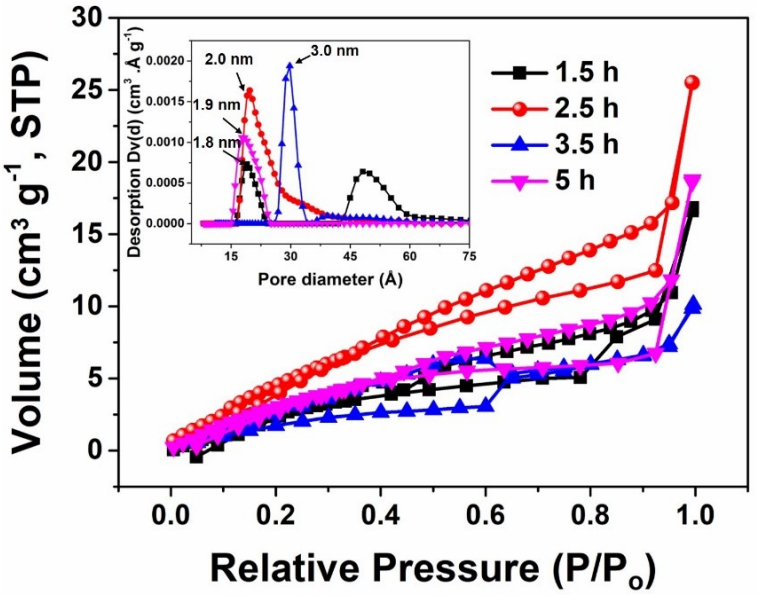

Figure S14. N_2 adsorption-desorption isotherms and pore size distributions (inset) of CC@CoO@S-Co_3O_4 at different thermal time of 1.5 h, 2.5 h, 3.5h and 5h, respectively.

In terms of CC@CoO (**Figure S14**), ideal rectangular CV curves are observed without redox peaks. The areal specific capacitances (C_a) are calculated to be 288, 235, 199, 141 and 89 mF cm^{-2} when the current density was increased from 1 to 20 mA cm^{-2}. The C_a value can

be retained at 30.9% when the current density is at 10 mA cm^{-2}.

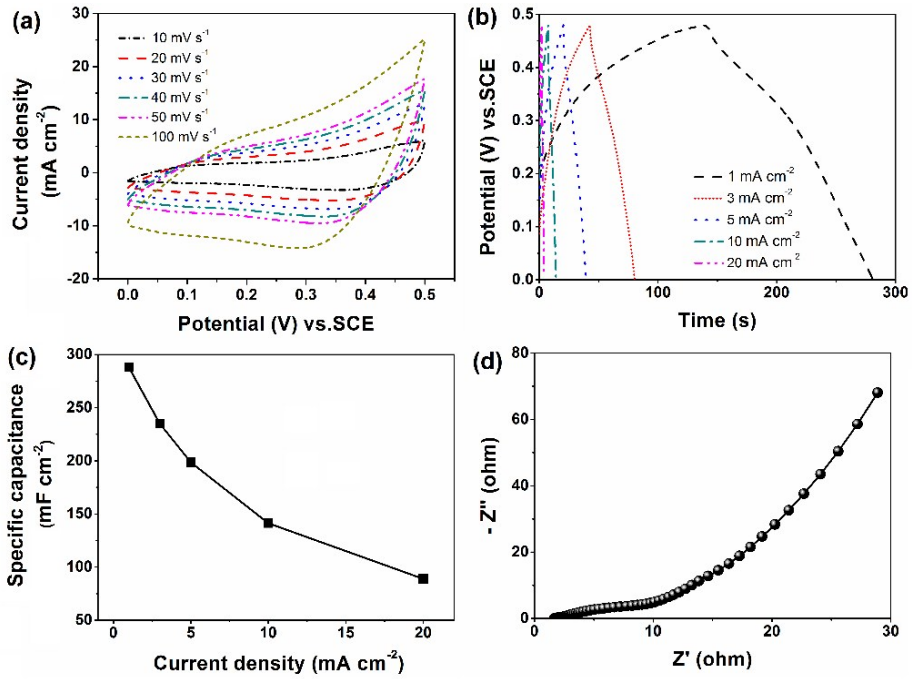

Figure S15. The electrochemical properties of CC@CoO using a three-electrode cell in 2 M KOH solution. (a) typical CV curves at different scan rates (10-100 mV s^{-1}), (b) Galvanostatic charge/discharge curves (1-20 mA cm^{-2}), (c) specific areal capacitance calculated from CP curves as a function of current density and (d) Nyquist impedance plots.

Ideal rectangular CV curves are also observed without redox peaks for CC@CoO@ZIF-67 electrode (**Figure S16**). The areal specific capacitances (C_a) are calculated to be 292, 256, 227, 164 and 86 mF cm^{-2} when the current densities are increased from 1 to 20 mA cm^{-2}. The C_a value can be retained at 29.5% when the current density is at 10 mA cm^{-2}.

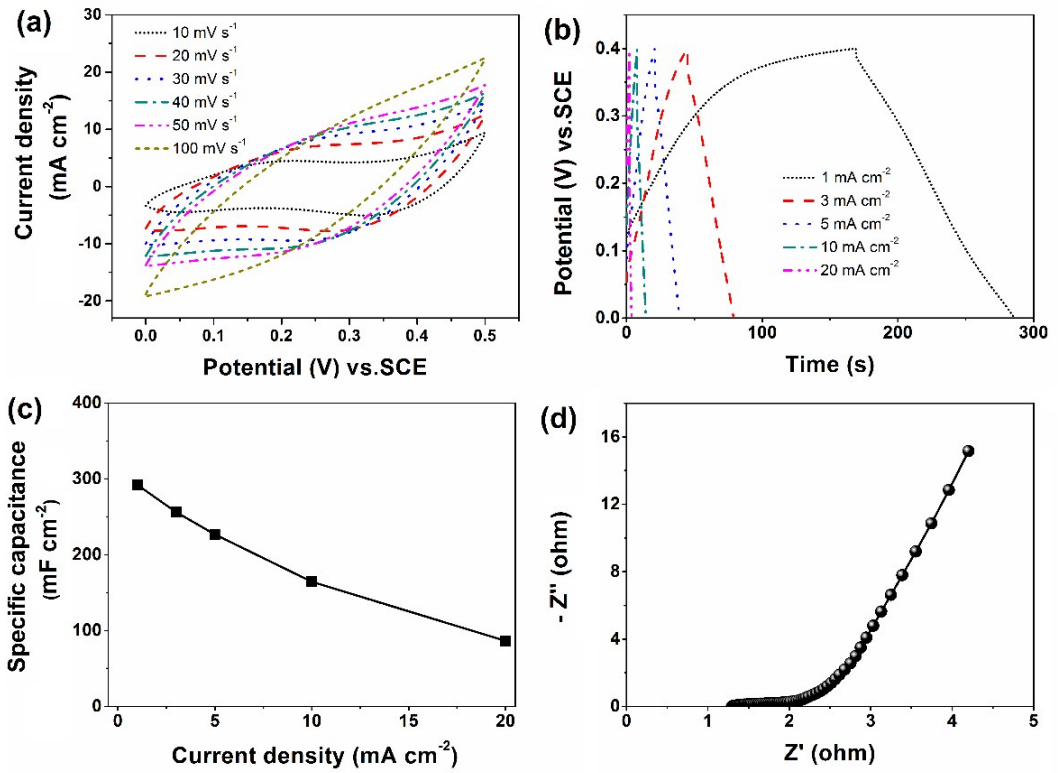

Figure S16. The electrochemical properties of CC@CoO@ZIF-67 using a three-electrode cell in 2 M KOH solution. (a) typical CV curves at different scan rates (10-100 mV s^{-1}), (b) Galvanostatic charge/discharge curves (1-20 mA cm^{-2}), (c) specific areal capacitance calculated from CP curves as a function of current density and (d) Nyquist impedance plots.

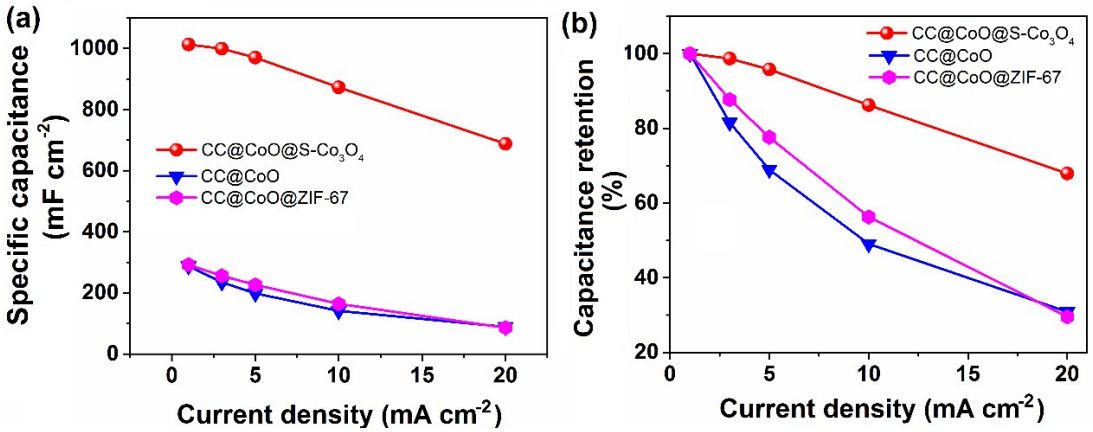

Figure S17. (a) Specific areal capacitance calculated from GCD curves and the retention value as a function of current density for CC@CoO, CC@CoO@ZIF-67 and CC@CoO@S-Co_3O_4; (b) Capacitance retention as a function of current density for CC@CoO, CC@CoO@ZIF-67 and CC@CoO@S-Co_3O_4.

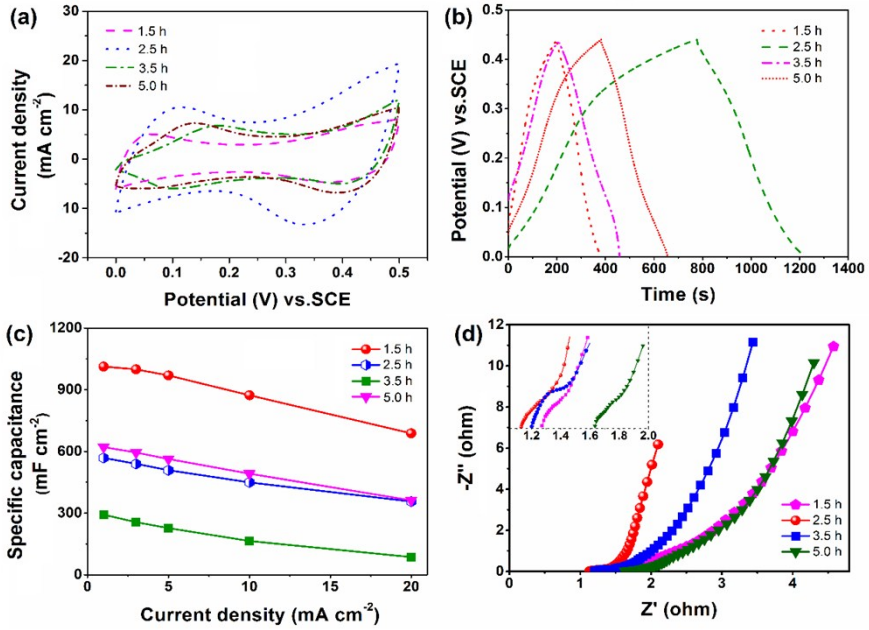

Figure S18. Comparison study of electrochemical properties for hybrids from different thermal times using a three-electrode cell in 2 M KOH solution. (a) Typical CV curves at 10 mV s^{-1} scan rate, (b) GCD curves at 1 mA cm^{-2} current density, (c) specific areal capacitances calculated from GCD curves as a function of current density and (d) Nyquist impedance plots.

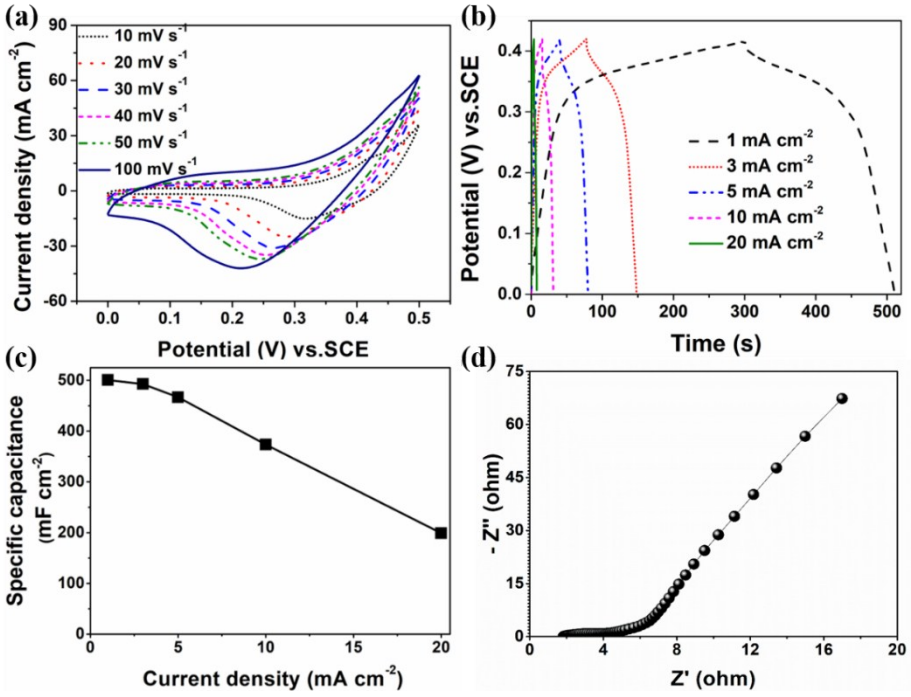

Figure S19. The electrochemical properties of CC@CoO@Co_3O_4 using a three-electrode cell in 2 M KOH solution. (a) typical CV curves at different scan rates (10-100 mV s^{-1}), (b) Galvanostatic charge/discharge curves (1-20 mA cm^{-2}), (c) specific areal capacitance calculated from CP curves as a function of current density and (d) Nyquist impedance plots.

Table S1. Comparison energy storage performance with representative cobalt oxides-based free-standing electrodes from literatures.

Electrodes	Specific capacitance	Rate capability	Cycles stability	Ref.
[a]CC@Co_3O_4	900 F g^{-1} (10 A g^{-1}) 0.225 mF cm^{-2}	58.7% (160 A g^{-1})	Not mentioned	S2
[b]Co_3O_4/GF	402 F g^{-1} (1 A g^{-1})	85.3% (20 A g^{-1})	84.3% (2 A g^{-1}, 3000)	S4
[c]Co_3O_4/rGO/CNTs	378 F g^{-1} (2 A g^{-1})	78% (8 A g^{-1})	Not mentioned	S5
Co_3O_4 grown on Ni foam	460 F g^{-1} (1 A g^{-1})	74.5% (5 A g^{-1})	Not mentioned	S6
[a]Co_3O_4@Fe_2O_3 on CC	245 mF cm^{-2} (1 mA cm^{-2})	46.1% (6 mA cm^{-2})	69% (60 mV s^{-1}, 1000)	S7
[d]G@Co_3O_4/NF (0.33 mg cm^{-2})	0.67 F cm^{-2} (1.0 mA cm^{-2})	108.9% (16 mA cm^{-2})	104% (1.0 mA cm^{-2}, 1000)	S8
3D graphene/Co_3O_4	768 F g^{-1} (10 A g^{-1})	59.4% (30 A g^{-1})	Not mentioned	S9
[e]Co_3O_4/GN/BC (9.61 mg cm^{-2})	12.25 F cm^{-2} 1274.2 F g^{-1} (3 mA cm^{-2})	84.9% (50 mA cm^{-2})	96.4% (50 mA cm^{-2}, 20000)	S10
CC@CoO@S-Co_3O_4 (1.013 mg cm^{-2})	1013 mF cm^{-2} (1 mA cm^{-2}) 1000 F g^{-1} (0.99 F g^{-1})	67.8% (20 mA cm^{-2})	67.7% (5 mA cm^{-2}, 5000)	Our work

Note: [a]CC, carbon cloth; [b]GF, graphene film; [c]rGO, reduced graphene oxide; [c]CNTs, carbon nanotubes; [d]G, graphene; [d]NF, nickel foam; [e]GN, graphene; [e]BC, bacterial cellulose.

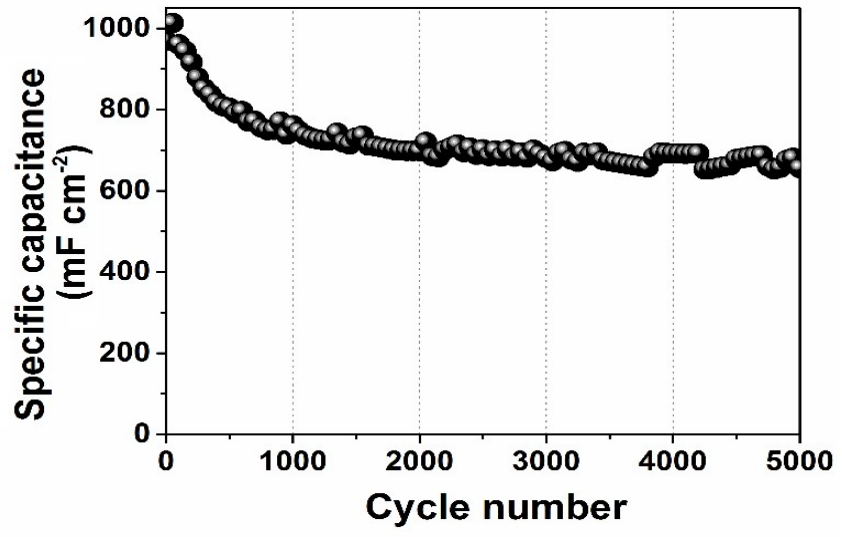

Figure S20. Long-term cycles performance for CC@CoO@S-Co_3O_4 at 5 mA cm^{-2}.

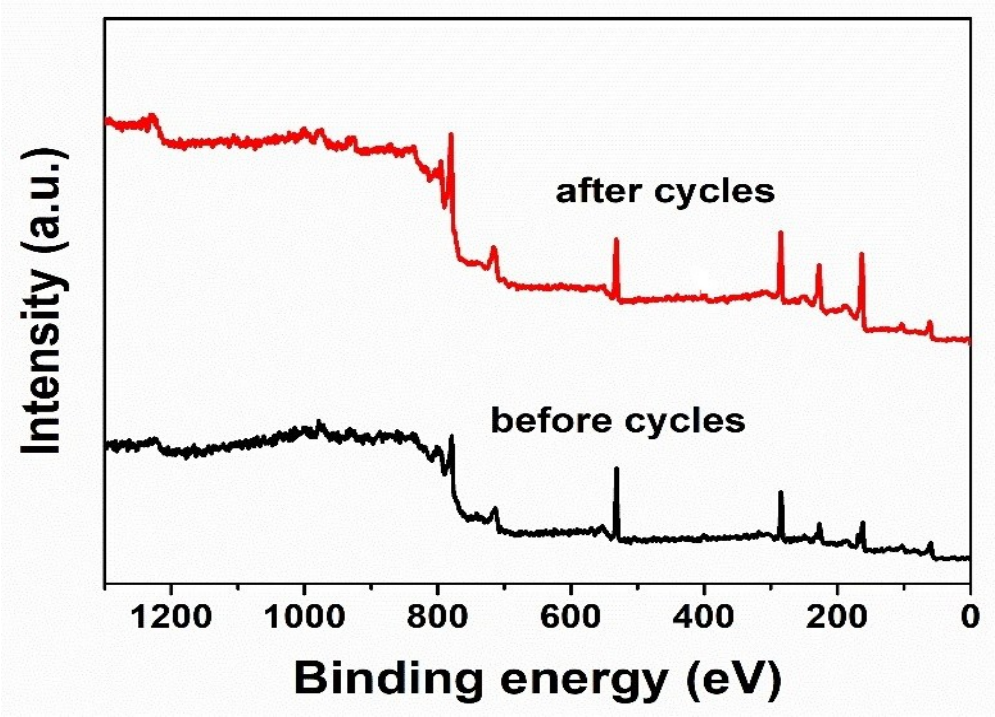

Figure S21. Full survey XPS spectra for CC@CoO@S-Co_3O_4 before and after cycles.

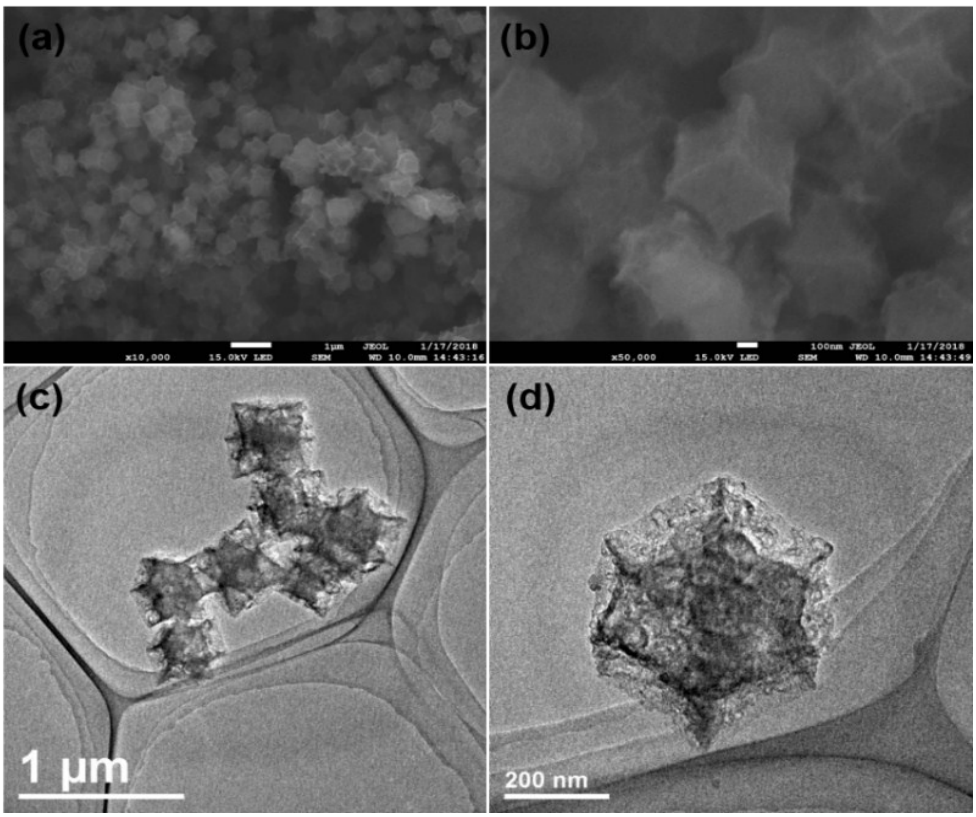

Figure S22. (a,b) SEM images and (c,d) TEM images of ZIF-67 derived carbons.

As shown in **Figure S22**, ZIF-67 derived cathode materials retain dodecahedra morphology, along with a diameter of 500 nm. Moreover, the pyrolysis process and the etching of Co ions lead to hollow interior voids. The Raman spectra give the distinct peaks for G band and D band without the peaks for metal-carbon bond (**Figure S23**). Therefore, ZIF-67 derived cathode materials are hollow carbon-based dodecahedra.

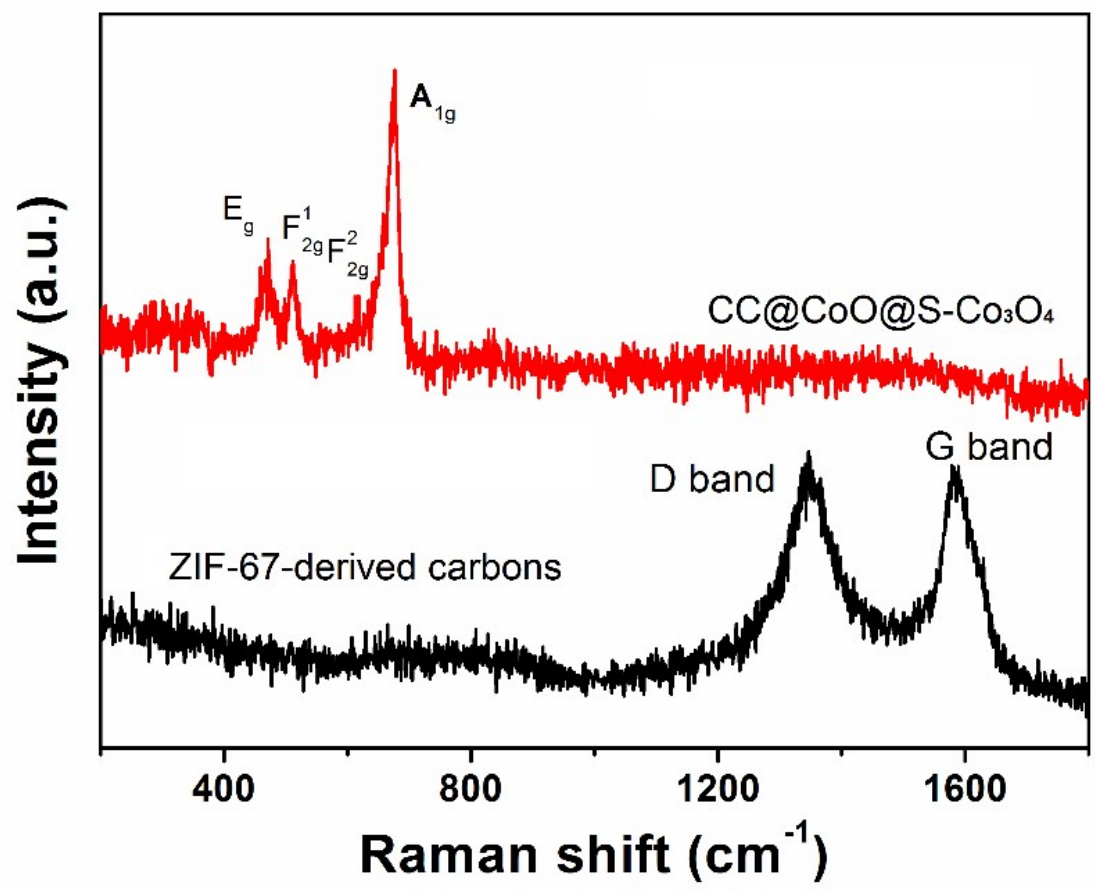

Figure S23. Raman spectra for CC@CoO@S-Co_3O_4 and ZIF-67-derived carbons.

The electrochemical performance was evaluated in a three-electrode cell in 2 M KOH solution. The CV curve shape maintains unchanged toward the increased scan rates. The areal specific capacitance can reach as high as 430 mF cm^{-2} at a current density of 1 mA cm^{-2}, suggesting that the nanoporous carbons are promising cathode materials (**Figure S24**).

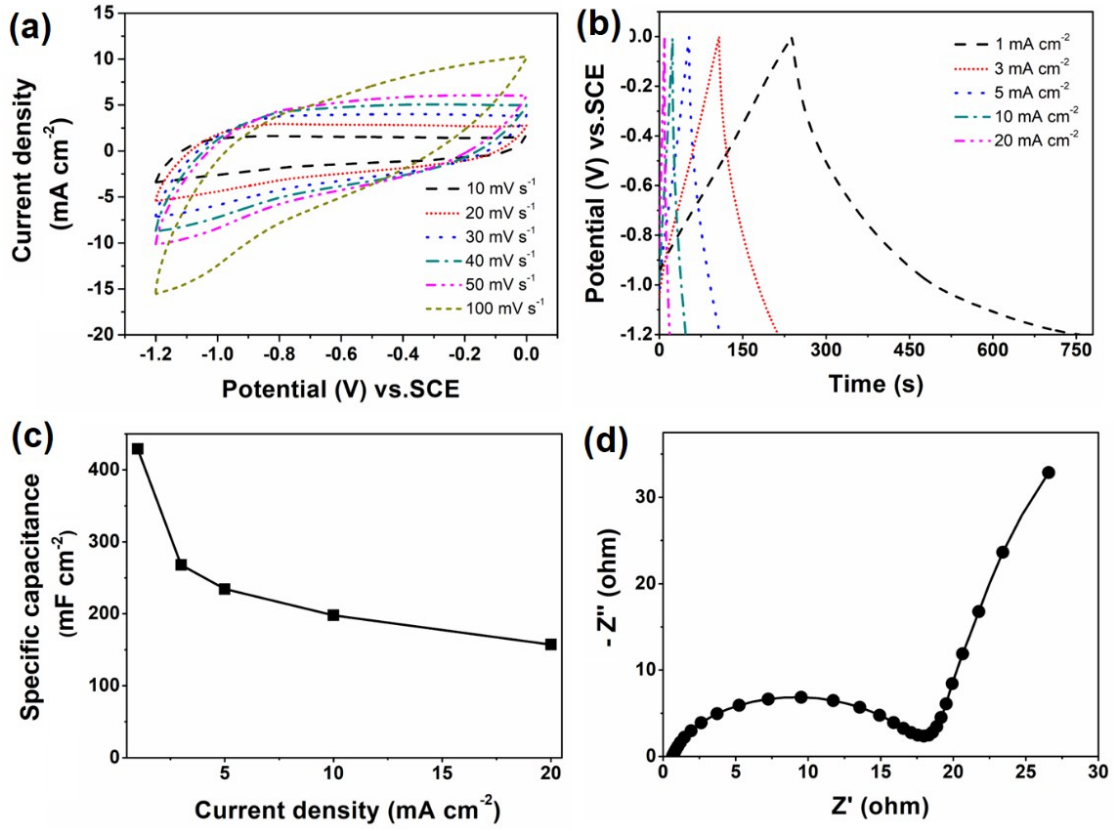

Figure S24. The electrochemical properties of ZIF-67-derived carbons using a three-electrode cell in 2 M KOH solution. (a) typical CV curves at different scan rates (10-100 mV s^{-1}), (b) Galvanostatic charge/discharge curves (1-20 mA cm^{-2}), (c) specific areal capacitance calculated from CP curves as a function of current density and d) Nyquist impedance plots.

Reference

(S1) S. Zhao, J. Guo, F. Jiang, Q. Su, J. Zhang, G. Du, *J. Alloy. Compd.* 2016, **655**, 372-377.

(S2) C. Guan, W. Zhao, Y. Hu, Z. Lai, X. Li, S. Sun, H. Zhang, A. K. Cheetham, J. Wang, *Nanoscale Horizons* 2017, **2**, 99-105.

(S3) D. Feng, Y. Song, Z. Huang, X. Xu, X. Liu, *J. Power Sources* 2016, **324**, 788-797.

(S4) D. Xiong, X. Li, Z. Bai, J. Li, H. Shan, L. Fan, C. Long, D. Li, X. Lu, *Electrochimica Acta* 2018, **259**, 338-347.

(S5) C. Yuan, L. Yang, L. Hou, J. Li, Y. Sun, X. Zhang, L. Shen, X. Lu, S. Xiong, X. W. Lou, *Adv. Funct. Mater.* 2012, **22**, 2560-2566.

(S6) X. Fan, W. Chen, S. Pang, W. Lu, Y. Zhao, Z. Liu, D. Fang, *Chem. Phys. Lett.* 2017, **689**, 162-168.

(S7) F. Yang, K. Xu, J. Hu, *J. Alloy. Compd.* 2017, **729**, 1172-1176.

(S8) H. Zhang, Y. Zhou, Y. Ma, J. Yao, X. Li, Y. Sun, Z. Xiong, D. Li, *J. Alloy. Compd.* 2018, **740**, 174-179.

(S9) X. Dong, H. Xu, X. Wang, Y. Huang, M. B. Chan-Park, H. Zhang, L. Wang, W. Huang, P. Chen, *ACS Nano*, 2012, **6**, 3206-3213.

(S10) R. Liu, L. Ma, S. Huang, J. Mei, E. Li, G. Yuan, *J. Phys. Chem. C* 2016, **120**, 28480-28488.